AIAA JOURNAL
Vol. 40, No. 3, March 2002

High Subsonic Jet Experiments: Turbulence and Noise Generation Studies

S. Narayanan*
United Technologies Research Center, East Hartford, Connecticut 06108
T. J. Barber†
University of Connecticut, Storrs, Connecticut 06269
and
D. R. Polak‡
United Technologies Research Center, East Hartford, Connecticut 06108

Experimental results from exploring the flowfield and noise generated by turbulent, high subsonic, single-stream jets are presented. We study the nature and directly measure the distribution of subsonic jet noise sources and attempt to establish their connection to some of its turbulence characteristics. Detailed measurements of the jet turbulence characteristics and of the spatial distribution of noise sources (using a linear phased array) are performed for an $M_j = 0.6$, $Re_D \cong 10^6$ isothermal jet. Noise source distributions are investigated for a wide range of jet Mach numbers ($0.5 \leq M_j \leq 0.9$) with and without heating ($T_j = 80$, 1000°F). The turbulence and source distribution measurements provide a unique experimental database for high subsonic turbulent jets with which to validate aeroacoustic prediction models. Key observations and conclusions of this exploration are 1) peak jet noise sources (dominant in the aft angle range $110 < \theta < 150$ deg) occur near the time-averaged potential core end of the jet; 2) there is a general trend of low-frequency noise sources being located downstream and high frequency noise sources being located close to the nozzle exit plane; 3) the jet turbulence equilibrates far downstream of the potential core end (beyond 10 jet diameters), where noise generation is relatively insignificant; and 4) the turbulence intensities reach a maximum near or after the potential core end inside the shear layer, displaying significant anisotropy.

Nomenclature

a	=	speed of sound
b	=	jet half width
D	=	diameter of nozzle
f	=	frequency, Hz
G	=	power spectral density
k	=	turbulent kinetic energy
M	=	Mach number
Re	=	Reynolds number
Sr	=	Strouhal number, fD/U
T	=	temperature
U	=	longitudinal velocity
u'	=	turbulence intensity
$u'v'$	=	component of Reynolds stress
x	=	axial coordinate, along jet axis
y	=	radial/transverse coordinate
δ^*	=	boundary-layer displacement thickness
θ	=	observer angle, referenced to upstream
θ_e	=	exit boundary layer momentum thickness

Subscripts

amb	=	ambient
cl	=	centerline
j	=	jet exit condition
uu	=	longitudinal velocity component fluctuation (used for velocity spectra amplitudes)

Received 11 March 2001; revision received 25 August 2001; accepted for publication 30 August 2001.

*Research Engineer, Systems Department. Member AIAA.
†Professor, Mechanical Engineering Department. Associate Fellow AIAA.
‡Research Engineer, Systems Department. Member AIAA.

I. Introduction

WHEREAS the study of generation of noise from turbulent jets has received widespread attention owing to its practical relevance in commercial aircraft applications (e.g., see Tam[1]), the fundamental mechanisms underlying the generation of jet noise remain poorly understood. Figure 1 shows a schematic of the flowfield in a top-hat profile, turbulent jet with organized (spatially coherent) motion, and disorganized random (fine-scale) turbulence, which are typical of the near-field jet evolution and the associated turbulence generation. However, it is unclear as yet how such organized and disorganized motions affect the far-field noise generation in high subsonic jet flows.

Computational techniques for aeroacoustics, capable of resolving flowfield details simultaneously with noise source generation and radiation (e.g., see Freund[2]), continue to suffer from the lack of predictions at realistic Mach and Reynolds numbers. On the other hand, state-of-the-art experimental techniques (also typically limited to low Reynolds number Re, Mach number M, and temperature) are limited in the spatiotemporal resolution needed to resolve the flowfield details (from which to compute or estimate the acoustics). Significant advances have been made on the computational[1] and experimental[3,4] fronts, enabling more detailed exploration of the noise generation process in high subsonic jets.

This study is a follow on to the one reported by Simonich et al.,[5] where an extensive aeroacoustic database regarding the time-averaged characteristics of high subsonic jet flowfields and the associated far-field acoustics were discussed. Here, we report an experimental investigation aimed at further exploring the turbulent flowfield and noise source distributions in turbulent high subsonic jets. Although the experimental data compiled is far from being comprehensive, we wish to gain some preliminary insight into the noise generation process and their implications for modeling jet noise. With significant advances in experimental diagnostics, measurements of turbulence statistics more directly relevant to noise generation, such as the two-point turbulence correlations, are now becoming feasible and will be needed for high subsonic jet noise model development and validation. The availability of such a unique database in high-Reynolds-number, turbulent, high-Mach-number

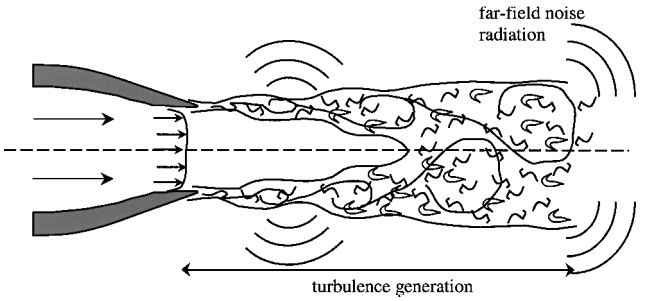

Fig. 1 Flow schematic of the turbulent jet.

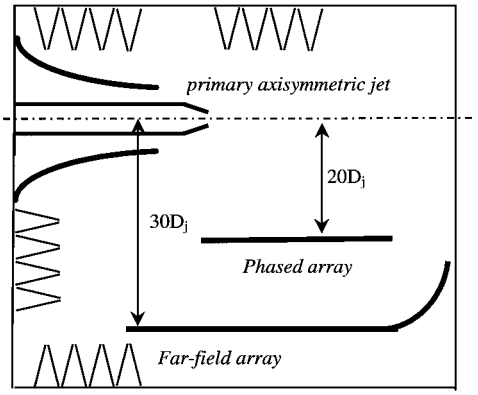

Fig. 2 Experimental facility schematic displaying jet exit, anechoic chamber, and acoustic measurements (near and far field).

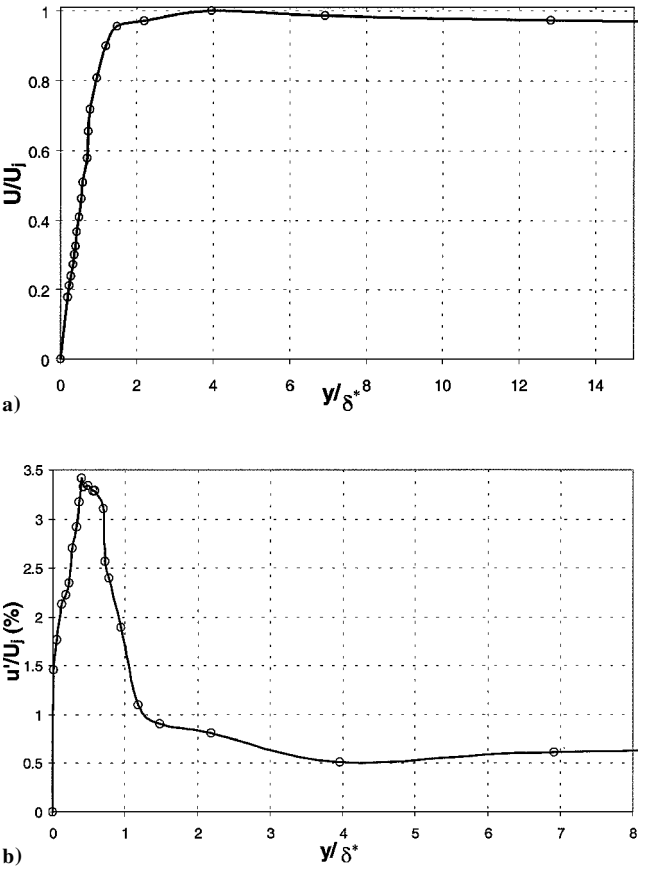

Fig. 3 Boundary-layer profile of longitudinal component of velocity at nozzle exit for $M_j = 0.6$ jet, showing a) mean and b) turbulence intensity.

jets is believed to be essential for validating high-fidelity computations, for example, direct numerical simulations and large-eddy simulations, as well as for mechanistic model development. A critical objective of this study is also to interrogate the nature of the jet near-field turbulence and source distributions in the light of assumptions made in various aeroacoustic theories and models.

II. Experimental Facility and Instrumentation

The experiments were conducted in a 82.27-mm axisymmetric, single-stream circular jet housed in a large anechoic chamber at the United Technologies Research Center (UTRC) with a coflow capability for simulating flight effects; see facility schematic in Fig. 2 (further details may be found elsewhere[5]). Single hot-wire and hot-film probes (TSI 1210-T2 and TSI 1210-20, respectively) were used to explore the turbulence characteristics in the near field of an $M_j = 0.6$, $Re_{Dj} = 1 \times 10^6$, top-hat profile jet at room temperature. Dual TSI hot-film sensors were used as well for surveying the degree of anisotropy in the flow. Hot-wire probes were employed for high-frequency response measurements, for example, turbulence spectra surveys, and the more robust hot-film probes were used for time-averaged measurements. The nozzle exit plane boundary layer was confirmed to be fully turbulent with nearly 0.5% freestream turbulence intensity levels, up to 3.5% peak turbulence intensity levels, broadband velocity spectra, and $Re_{\theta e} > 2000$ (the Reynolds number based on the exit momentum thickness). Figure 3 shows the mean velocity and turbulence intensity profiles measured across the boundary layer at the nozzle exit plane, showing peak turbulence intensity within one displacement thickness δ^* of the boundary layer (as expected for turbulent boundary layers). Boundary-layer spectra were measured to confirm the absence of dominant facility related tones or disturbances. Total pressure and temperature and static pressure measurements, as well as far-field acoustics measurements, are reported by Simonich et al.[5]

A 36-microphone, linear phased array (developed at UTRC) was used for source localization in both cold and heated jet flows. The sources were assumed to be radially compact, but axially noncompact, producing an equivalent noise source distribution on the jet centerline. For the simple delay-and-sum beamformer, the output of time-delayed sensor measurements are summed, with the delays a function of focus position and sensor location, to form an estimate of the source distribution.[6] In practice, the processing is usually performed in the frequency domain, where phase shifts are used instead of time delays. When a source exists at the focus position, the signals add coherently to produce an enhanced signal; whereas when the focus position contains no source, the signals add incoherently. The performance of the simple delay-and-sum beamformer can be significantly improved by weighting the microphone signals before summation. In the array processing developed and used here, the optimum sensor weighting is determined for each focus position by minimizing the measured source contribution from all positions away from the focus position relative to the source contribution from the focus position itself. This novel processing technique attempts to enhance significantly the spatial resolution for locating noise sources while minimizing sidelobe level (away from the source peak) and is discussed further elsewhere.[7]

The array was positioned parallel to the jet aerodynamic centerline (aligned to within 1 deg) at a distance of 1.65 m ($=19.9D_j$). Acoustic foam treated all exposed portions of the array beam. The microphone sensors were positioned in a linear geometry using an orthogonal restricted basis,[8] where the first 18 microphones were separated by 0.007 m and the last 18 were separated by 0.143 m. The actual microphone positions were measured with a micrometer with an error of less than 0.5 mm. The total array aperture was 2.70 m ($=32.6D_j$), and the first microphone was at $\theta = 85$ deg, whereas the 36th microphone was at $\theta = 147$ deg. Because source directivity was not accounted for in the processing, the measurements can be considered a weighted average over the subtended θ. Omnidirectional sources have also been assumed in other jet noise source localization studies.[9,10] Furthermore, the array geometry was designed so that the 18 closely spaced microphones, primarily responsible for localizing high-frequency sources, were all nearly 90-deg aligned with where the high-frequency sources were expected, namely, upstream. Similarly, the 18 farther-spaced microphones, primarily responsible for localizing low-frequency sources, were all aligned approximately 90 deg with respect to where the lower frequency sources were expected, namely, downstream.

Condenser microphones (B&K 4939) were used in the array. Each data channel was bandpass filtered between 0.5 and 40 kHz and simultaneously acquired at 100 kHz with 16-bit resolution. The source distributions were produced using 2.5 s of data, which was sufficient because the distributions converged to better than 0.5 dB at all frequencies after 2.0 s of data. The amplitude response of the data acquisition system was calibrated by a pistonphone at 1 kHz. Because typical pretest and posttest results differed (by less than 0.2 dB) for each sensor, the mean of the amplitude corrections were applied to the raw data before processing. The phase response of the data acquisition system was measured by injecting broadband noise into the microphone preamplifiers simultaneously. The maximum phase difference of any two channels at any frequency from 1 through 33 kHz was found to be less than 5 deg. Phase corrections were not applied to the raw data.

The performance of a phased array is measured in terms of its sidelobe rejection and beamwidth when attempting to resolve a point source. The former determines the instrument's dynamic range, whereas the latter determines the spatial resolution (Fig. 4). The sidelobe and beamwidth can be determined by scanning a region of space containing a point source. Although the theoretical performance of a processing algorithm can be determined by introducing a delta function into the processing, the preferred approach is to use an in situ experimental technique because this includes the effects of imperfect sensors, imperfect instrumentation, and nonideal acoustic propagation in the test chamber. For the UTRC array, a 5-mm-diam air jet with its axis orthogonal to the array dimension was used as a broadband point source. Figure 5 shows a summary of the array performance, showing that, at frequencies greater than 1.5 kHz, the new beamforming algorithm achieves a 20-dB or better sidelobe (SL) rejection with a 5-deg beamwidth (enabling an accurate source magnitude and location method). For the jet noise source measurements reported here, accounting for the spectral averaging errors (typically minimized by the use of a large data sample) and those from the array processing, the source amplitudes measured are considered to be accurate to within ± 1 dB. The source peak location (for any given frequency band) are measured reliably to within $1 D_j$. Flow refraction effects due to gradients within the primary jet were ignored for the array processing because they are expected to introduce relatively smaller errors in the source location estimate. Further discussion of the array hardware, instrumentation, validation, and processing details are presented elsewhere.[7]

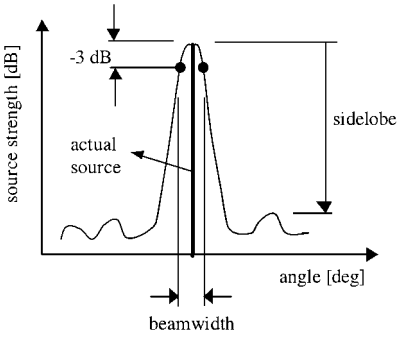

Fig. 4 Schematic of a phased array SL and beamwidth.

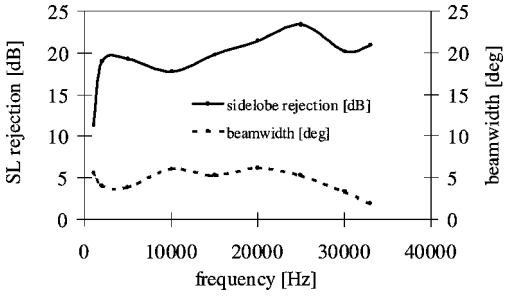

Fig. 5 SL rejection and beamwidth of UTRC linear phased array.

III. Experimental Characterization of Jet Noise Sources

A detailed benchmark aerodynamic and acoustic database was generated for a high-speed, high-Reynolds-number, heated and cold round jets (see Simonich et al.[5]). Certain passive noise control concepts, for example, the use of tabs, a flexible string, were investigated and produced mixed results for far-field noise reduction. Generally, noise intensities in low-frequency ranges were found to be reduced, whereas the intensity at high frequencies saw an increase. These results suggest source modification as a result of certain device/control-induced flow changes. However, no evidence or insight into the flow processes that led to the modification of the noise spectra was possible using the conventional measurement techniques, motivating the following exploration of the noise generation process. To complement the database, a detailed set of experiments were performed to 1) locate the noise sources and 2) explore the turbulence characteristics relevant to noise generation.

A. Jet Noise Source Location and Distribution

A 36-microphone linear phased array was used to examine the source distribution in the single-stream jet. Figure 6 shows the source

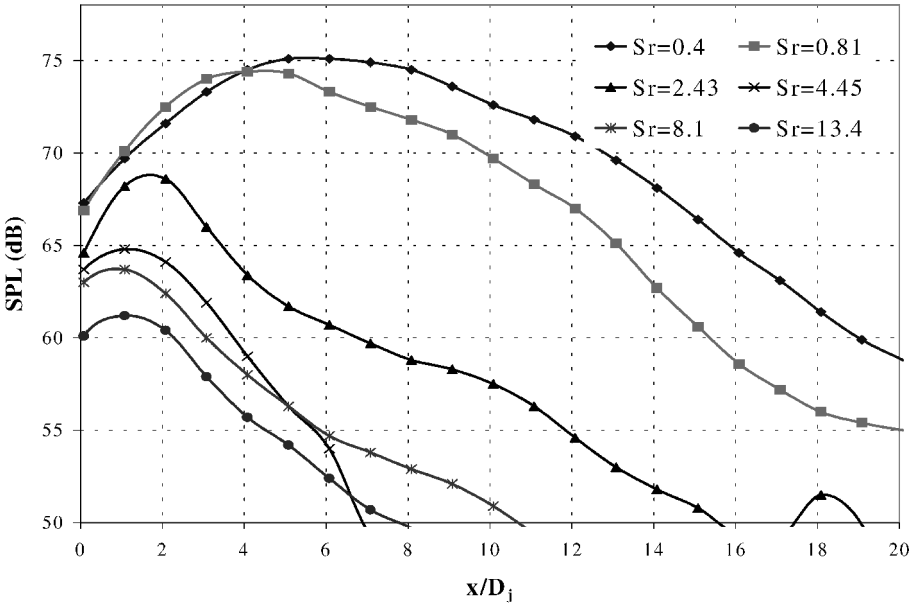

Fig. 6 Source distribution for $M_j = 0.6$ ($T_{ambient} = 83°$F), measured using linear phased array, for center frequencies $f = 1$, 2, 5, 11, 20, and 33 kHz (using constant bandwidth of 195 Hz) corresponding to $0.4 < Sr_D < 14$.

distributions (processed in narrowband) for a cold, $M_j = 0.6$ jet for several frequencies in the range $1 < f < 33$ (kHz). The frequency of 1 kHz for $M_j = 0.6$, cold jet corresponds to $Sr_D = 0.4$ and peaks near $x/D_j = 6$. The nondimensional Strouhal number is defined as $Sr_D \equiv f D_j / U_j$. We will see in the next section that this is located where the time-averaged potential core end resides. This is also the frequency band around which the jet noise peaks in the far-field acoustic spectra in aft angles, that is, $100 < \theta < 140$ deg (Fig. 7). As the noise radiation frequency increases, the corresponding source location peak moves upstream, reaching $x/D_j = 1$ for the high frequencies ($f > 10$ kHz, that is, $Sr_D > 4$ for $M_j = 0.6$, cold jet). This trend is evident in Fig. 6, showing the source distributions overlaid for different frequencies for an $M_j = 0.6$, cold jet. (Note that the spatial resolution associated with the source distributions is $\Delta x/D_j = 1$, providing an upper bound on the uncertainty in the measured source peak location.)

These views match well with results presented from analytical and experimental studies,[9,11,12] and one can make similar observations as follows:

1) The main contribution to the noise intensity for low frequencies of $0.4 \le Sr_D \le 0.8$ occurs from the region $5 \le x/D_j \le 10$.

2) The main contribution to the noise intensity for high frequencies of $2 \le Sr_D \le 10$ occurs in the region $0 \le x/D_j \le 3$.

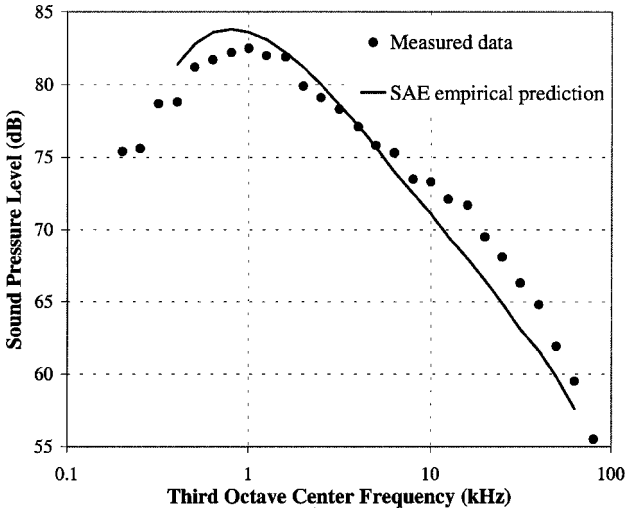

Fig. 7 Far-field third octave acoustic spectrum measured at a rearward angle of 150 deg to the upstream jet axis (compared with the Society of Automotive Engineers prediction).

3) The low-frequency noise generation region is spread over a large flow region, but its downstream ($x/D_j \ge 10$) contribution to the total noise is small.

4) The present data indicate a more rapid drop off at high frequencies compared to that in previous studies.[11,12]

5) In contrast to the present results (suggesting intense noise generation for $x/D_j < 10$), the lower frequency noise sources from previous analyses appeared to be much more distributed in the streamwise direction, remaining intense at farther downstream locations (perhaps due to larger uncertainties in the source locations and poorer source amplitude estimates).

The locations (x/D_j) of the peak noise sources occurring at various nondimensional frequencies of the noise source are shown in Fig. 8, with a logarithmic ordinate, for $M_j = 0.6$, 0.7, and 0.9 and $T_j = 80$ and 1000°F. The peak locations were extracted from the noise source distribution measured by the phased array. Although qualitative, the rough boundary drawn around the scattered data indicates a general trend for the location of the noise source peaks for cold as well as heated, single-stream jets over a range of M_j. These results are consistent with those reported in relatively lower M_j cold jets, using a different source localization technique,[13] where it was possible to locate the source peak locations but not their distributions. In particular, note that the noise source associated with the dominant frequency in the aft angle far-field noise spectra, corresponding to $Sr_D \approx 0.4$, is located near the end of the averaged potential core ($x/D_j = 6$). Note again that the linear phased array used here determines the source strength and distribution at a sideward angle of 90 deg. Whereas the source amplitudes are clearly higher at the rearward angles (because of the jet noise directivity), the location of the peak noise frequency is most reliably measured at the sideward angle (with minimal refraction effects). Recent experiments using a simpler source location technique,[14] but aimed at an angle of 150 deg relative to the upstream jet axis, also reveal the peak jet noise source location in an $M_j = 1.3$ jet to be between $5D_j$ and $11D_j$.

Figure 9 summarizes the source distribution pattern in the $M_j = 0.6$ jet as a function of Strouhal number Sr_D. The general trends of low-frequency noise sources being located downstream of the jet and high-frequency noise sources being located close to the nozzle exit plane are consistent (in low and high speed, and in cold and heated jets) with earlier observations. The turbulence characteristics associated with such source distributions are the subject of discussions in the forthcoming section. The source distribution for an $M_j = 0.9$ heated jet is shown in Fig. 10, displaying similar trends of downstream-located low-frequency sources and upstream-located high-frequency sources. However, the sources are distributed farther downstream for the heated jets compared to distributions for the cold jets. Source distributions from cold jets at other Mach numbers are similar in spatial extent to those for the $M_j = 0.6$ cold jet.

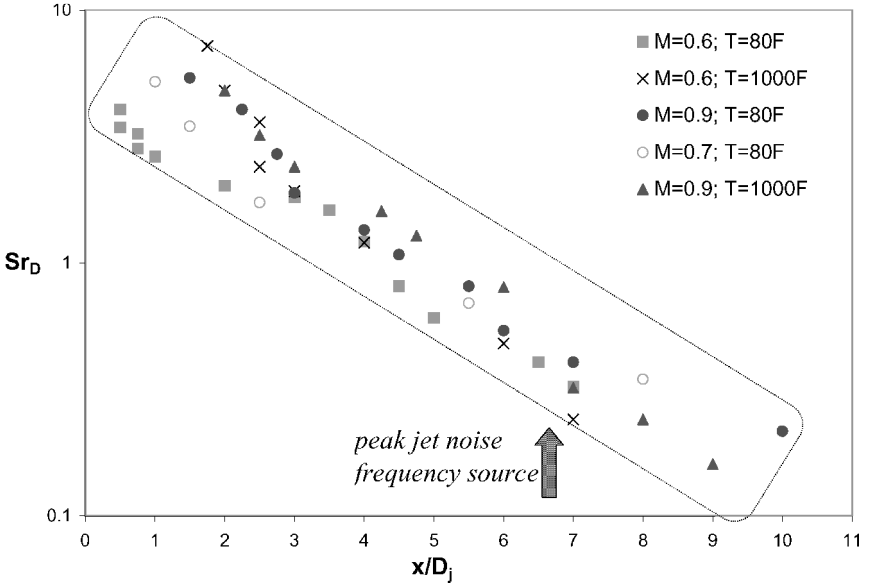

Fig. 8 Peak noise source locations as a function of the nondimensional downstream distance.

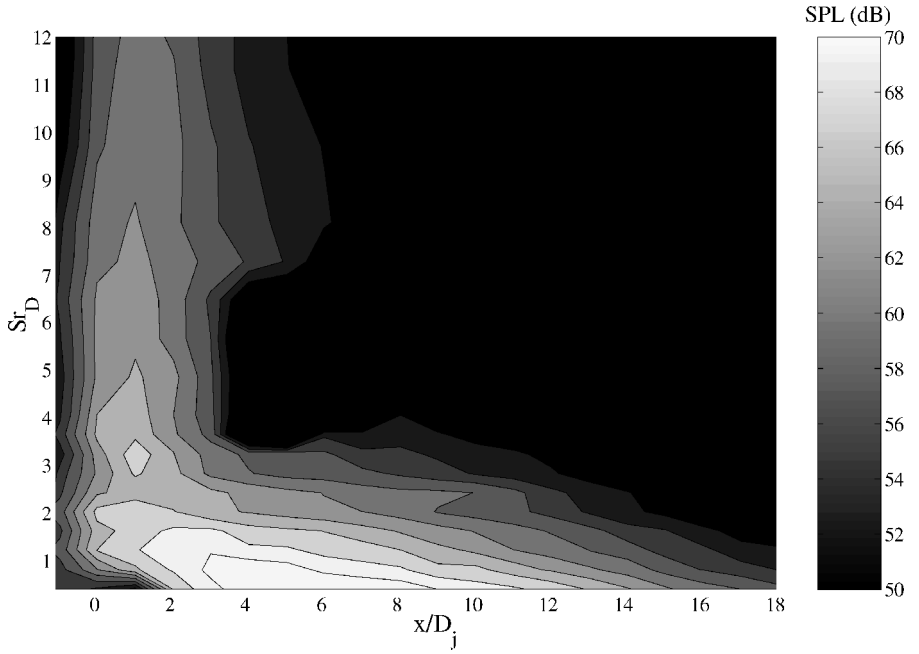

Fig. 9 Noise source distribution in $M_j = 0.6$ cold jet for $0.4 < Sr_D < 14$ (corresponding to $1 < f < 33$ kHz, using constant bandwidth of 195 Hz).

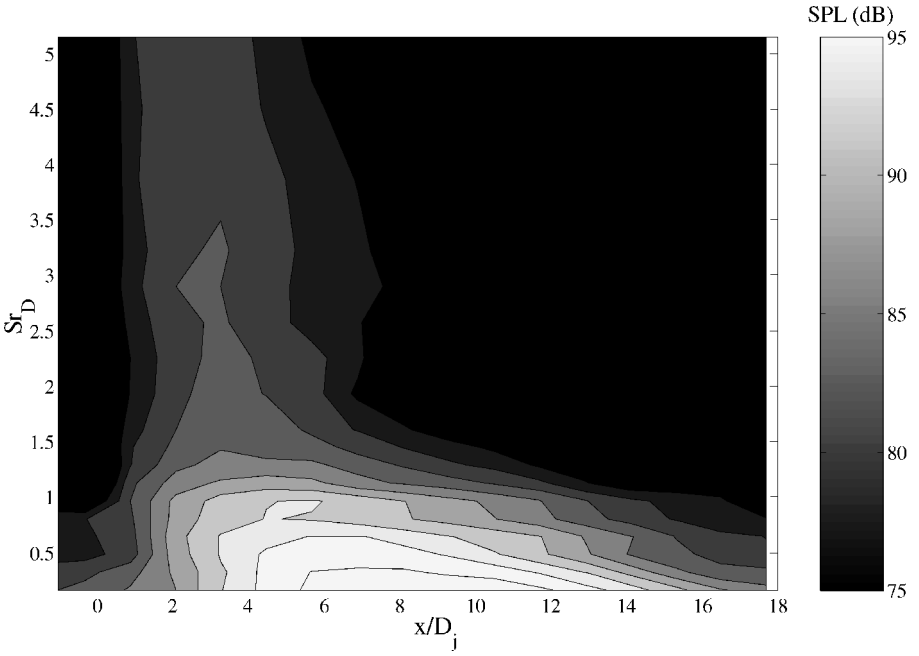

Fig. 10 Source distribution in $M_j = 0.9$, $T_j = 1000°$F jet for $0.15 < Sr_D < 6$ (corresponding to $1 < f < 33$ kHz, with constant bandwidth of 195 Hz).

The potential temperature-driven mechanisms responsible for the difference in the cold- and heated-jet source distributions are not yet well understood.

Figure 11 shows the sound power (in decibel) in the frequency band corresponding to $Sr_D = 0.4$ (the peak noise frequency band in far-field acoustic spectra) for a range of jet exit conditions, computed by spatial integration of the measured source distribution on the jet centerline. The constant slope for the cold and heated jets is evident, as is the difference in the intercepts (also see Tam[1]); further data for low Mach number heated jets are clearly needed to confirm this trend. Furthermore, the sound power level in the aforementioned frequency band is seen to scale as U_j^8, as expected for quadrupole type noise radiation. Here again, the levels are computed for a nominally sideward angle of 90 deg; the sound power levels are expected to be higher for aft angles (where the peak jet noise frequency appears to be dominant), but the suggested trend is not expected to change. Similar correlation of the sound power levels in a high-frequency band (not shown here), located closer to the nozzle exit plane, with the jet velocities indicates a scaling of neither U_j^6 (for dipole noise) nor of U_j^8 (expected for turbulence-generated quadrupole noise). This suggests the possibility of a combination of source types associated with near-nozzle high-frequency noise generation.[15] The generation of coherent vortices as a result of shear layer instabilities near the nozzle exit plane suggests noise radiation due to possibly two mechanisms: vortex–solid body interaction (as a dipole-type noise source) and vortex-generated turbulence (as a quadrupole-type noise source).

B. Near-Field Turbulence Characteristics of High-Reynolds-Number Jets

Hot-wire measurements of the mean and fluctuation velocities in the jet were performed. The jet Mach number, $M_j = 0.6$, is not believed to be high enough for compressibility effects to contaminate the hot-wire measurements. The objective of this study was to

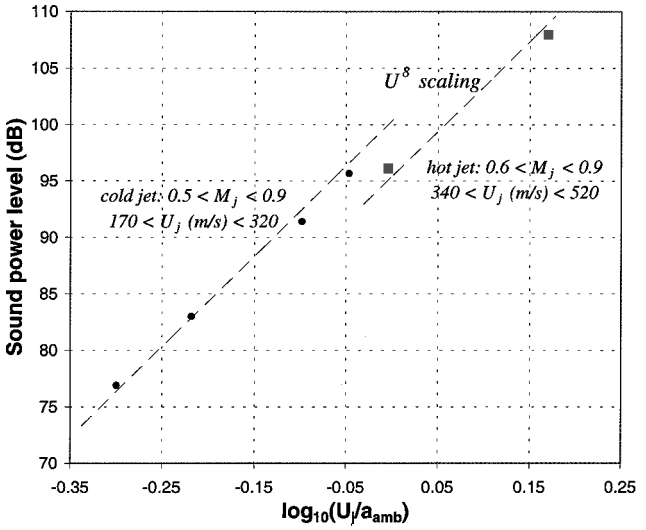

Fig. 11 Sound power level variation with jet exit velocity in the frequency band for peak jet noise generation, that is, $Sr_D \approx 0.4$, for cold ($T_j = 83°F$) and hot ($T_j = 1000°F$) jets.

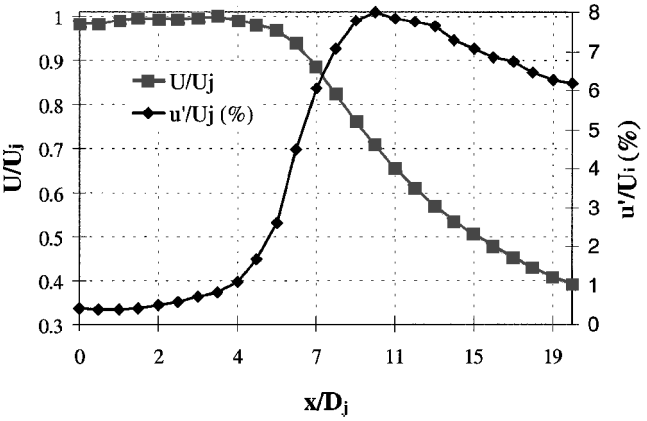

Fig. 12 Streamwise variation of longitudinal components of mean velocity and turbulence intensity on jet centerline (M_j = 0.6, $T_{ambient}$ = 83°F).

explore the time-averaged characteristics of a high subsonic jet (for which turbulence data are limited in the published literature) and to examine the implication of these results for noise prediction.

The normalized mean velocity and turbulence intensity on the jet centerline, obtained using a single hot-film probe for an $M_j = 0.6$ cold jet, are shown in Fig. 12. The displayed quantities have been normalized by the peak jet velocity (occurring near the nozzle exit plane). The end of the potential core (in a time-averaged sense) can be seen to be near $x/D_j = 4$. The mean velocity rapidly decays in the aerodynamic far field (proportional to $1/x$, as expected for a turbulent jet). The peak turbulence intensity on the jet centerline is seen to be reached near $x/D_j = 10$.

Radial mean velocity profiles for $M_j = 0.6$, at several streamwise locations, are shown in Fig. 13. The potential core is evident in the $x/D_j = 1$ profiles and barely visible in the $x/D_j = 4$ profiles. The mean velocity profiles are normalized by the local (in x) centerline mean velocity U_{cl}, as a function of the radial distance from the jet centerline line, normalized by the jet half width (for $M_j = 0.6$ data). The half width b is defined as the radial location where the local velocity reaches half of the centerline value. Self-similarity of the mean velocity profiles can only be discerned beyond $x/D_j = 10$.

Figure 14 shows the radial profiles for the turbulence intensity measured with the single sensor hot-film probe, displaying higher levels (compared to the centerline values) in the shear layer, as expected. Repeatability tests were conducted for the longitudinal turbulence intensity measurements providing error bounds of $\pm 1\%$. The peak seems to occur in a large region around $4 < x/D_j < 10$

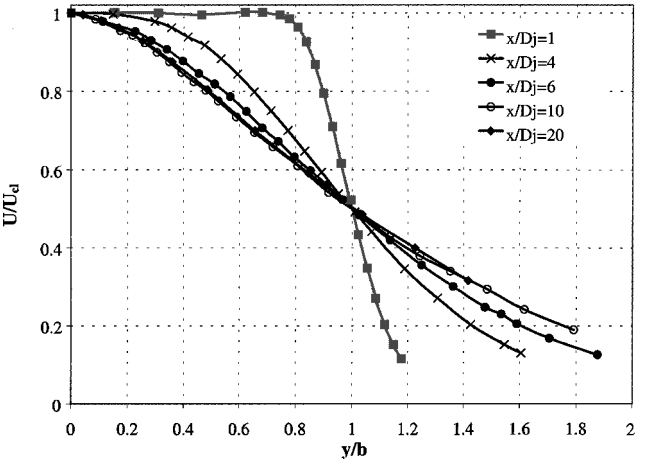

Fig. 13 Normalized mean longitudinal velocity profiles (for M_j = 0.6) at several streamwise locations.

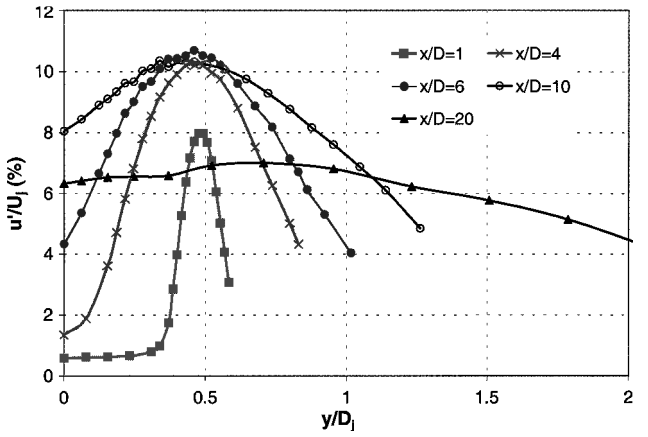

Fig. 14 Radial profiles of longitudinal turbulence intensity at different streamwise locations for M_j = 0.6 ($T_{ambient}$ = 83°F).

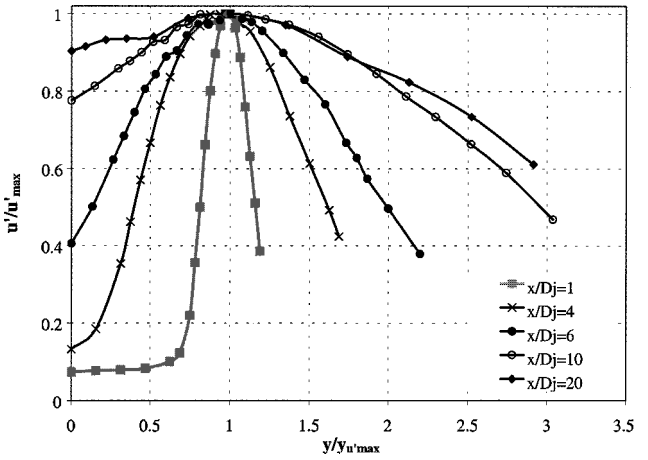

Fig. 15 Normalized radial profiles of longitudinal turbulence intensity at different streamwise locations for M_j = 0.6 ($T_{ambient}$ = 83°F) showing similarity of turbulence intensity profiles for $x/D_j \geq 10$.

close to the nozzle lip line. The normalized turbulence profiles using local variables, namely, the local peak turbulence intensity level u'_{max} and the peak level transverse location $y_{u'max}$, are shown in Fig. 15. A similar display method was used by Lau[16] to explore the universal distribution of axial turbulence intensity among various Mach number jets for a fixed streamwise location. Here, we investigate similarity among turbulence intensity profiles at various streamwise locations. No sign of self-similarity or universality for the turbulence intensity profiles is evident for $x/D_j < 10$ (as was the case for the mean velocity profiles). Several

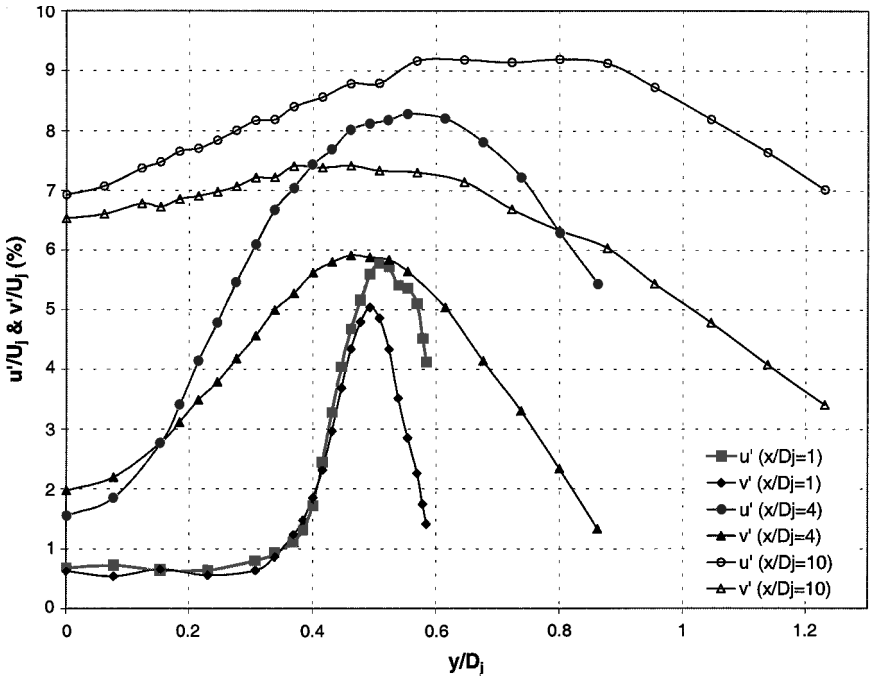

Fig. 16 Profiles of longitudinal and transverse turbulence intensities at various streamwise locations for $M_j = 0.6$ ($T_{\text{ambient}} = 83°$ F).

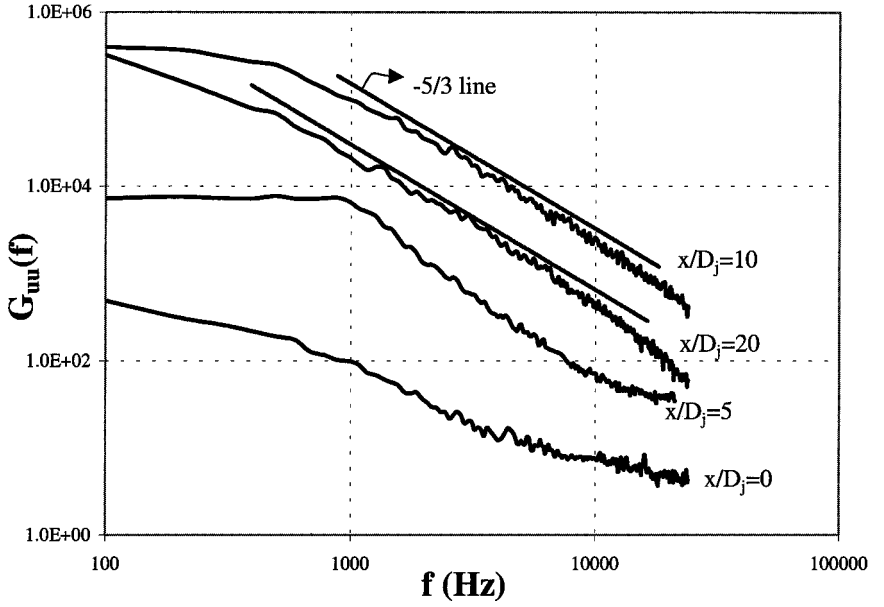

Fig. 17 Velocity spectra for $M_j = 0.6$ ($T_{\text{ambient}} = 83°$F) along jet centerline.

modeling approaches, therefore, wrongly seem to assume the jet turbulence to be self-similar in the most intense noise-generation flow region.

Significant anisotropy was also evidenced from measurements of the u' and v' component (Fig. 16, measured using a dual TSI hot-wire sensor), displaying nearly 30–40% difference in the peak levels within the near-field jet shear layer for $x/D_j \leq 10$. (Uncertainty errors in measuring the transverse component of turbulence intensity v' were found to be higher in the jet core, namely, $\pm 10\%$, due to low levels of its mean component inside the potential core, but these errors reduce significantly inside the shear layer.) However, the present measurements are not an adequate characterization of anisotropy in the flow. The measured degree of anisotropy, due to differences in the turbulence intensity amplitudes, does not include the discrepancies in the turbulence correlation length scales, also a source of anisotropy. Such anisotropy can have significant implications for noise source modeling. Consider the simplified case of axisymmetric turbulence, where the characteristics, that is, amplitude and correlation length, of the longitudinal component of turbulence is different from the other two components (which are believed to be similar. It has been shown that the noise generation is significantly altered by considering anisotropy in correlation lengths (e.g., see Goldstein and Rosenbaum[17] and Khavaran and Krejsa[18]). When axisymmetric turbulence was assumed and correlations derived from measurements in a $M_j = 0.3$ jet (Ref. 19) were used, Goldstein and Rosenbaum[17] showed that the sound intensity can be highly directional for correlation length anisotropy, producing nearly 3-dB increase in aft angle spectra (compared to that expected from assuming isotropic turbulence).

The time-averaged normalized Reynolds stress component profiles $\overline{u'v'}(y)$ were also measured (not shown here) at a few streamwise locations, showing that the peak of the $\overline{u'v'}$ Reynolds stress component is reached in the shear layer (near the nozzle lip line $y/D_j = 0.5$). The peak (indicative of regions of turbulence production) is, however, only reached for $x/D_j \geq 4$, coinciding with the flow region displaying the highest turbulence intensities.

The cited experimental surveys were also performed for an $M_j = 0.4$, single-stream, cold jet (not shown here), with similar trends and conclusions. The result of turbulence intensities reaching a peak in the shear layer farther downstream of the potential core end have implications for current aeroacoustic models, namely, those based on the use of Reynolds-averaged Navier–Stokes (RANS) simulations with turbulence modeling (e.g., Balsa et al.[19] and Tam and Auriault[20]). Such models predict noise source distribution based on flow region of intense turbulent kinetic energy, for example, scaling with $k^{7/2}$, which are located in the region where turbulence intensities are observed to be large. The observation of high-turbulence intensities near and farther downstream of the potential core end, extending from $4D_j$ to $12D_j$, suggests the location of the noise sources in that flow region. Our source localization measurements suggest that this is only partially true (see earlier section and results within). In particular, only the low-frequency noise sources (typically in the frequency range below where the peak of jet noise generation is evidenced in aft angle far-field acoustic spectra) are located beyond $x/D_j = 6$. A bulk of the noise generation (in particular at high frequencies) is in fact generated several jet diameters farther upstream than expected to be predicted by conventional models.

An investigation was conducted to determine the streamwise extent over which the jet turbulence equilibrates, that is, an inertial subrange in the spectra is evident. Figure 17 displays the velocity spectra $[G_{uu}(f)]$ obtained from time series recorded by a hot-wire probe at four streamwise locations on the jet centerline, namely, $x/D_j = 0$, 5, 10, and 20. Overlaid in Fig. 17 is also a $-\frac{5}{3}$ slope line, which is indicative of an equilibrated (Kolmogorov-type) inertial subrange. We find a reasonable indication of equilibrated turbulence, that is, observation of $-\frac{5}{3}$ slope over at least one decade only for $x/D_j \geq 10$, where the mean velocity profile also displays self-similarity (see earlier results). Velocity spectra for the upstream locations between $0 < x/D_j < 5$ were also obtained inside the turbulent shear layer, where more broadband behavior was noticed but evidence of equilibrated turbulence (in the form of a $-\frac{5}{3}$ slope) was absent. Current noise prediction models, for example, based on RANS computations,[19,20] assume that an equilibrium, isotropic turbulence model applies, for example, the k–ε model, for the noise producing flow region. The lack of equilibration in the flow region within $10D_j$ questions the validity of such models for noise prediction in the dominant noise producing jet region.

IV. Conclusions

The noise source distribution measurements combined with the turbulence measurements provide a unique (although preliminary) experimental database with which to validate jet noise prediction models, providing much needed insights into the noise-generation processes. The flow regions of peak turbulence levels in the shear layer (near the potential core end of the jet) correlate well with the band of frequencies in which the peak noise radiation in the far field (in rearward angles) is noticed. There exists, however, a significant portion of the noise spectrum originating from the near field of the jet (before the end of the potential core of the jet), where lower intensity, but practically relevant,[5] high-frequency sources are located. Note that high-frequency noise in model scale would translate in engine scale to sound generation at frequencies that would contribute the most to human hearing and annoyance.[5] The flow structure dynamics in this region and their connection to noise generation is yet to be explored in detail.

A majority of jet noise studies and associated prediction and noise reduction approaches have focused on peak jet noise generation mechanisms associated with the jet's aerodynamic far-field features (both at large as well as small flow scales). Consequently, turbulence generation near the end of the jet potential core and farther downstream has received the most attention. Although not responsible for peak noise generation, near-field high-frequency noise sources (in laboratory-scale experiments) become relevant in full-scale engine noise characteristics.[5] The ultimate noise reduction benefits are realized as a result of an integrated effect over a broad range of frequencies, requiring control of noise generation at low and high frequencies, for example, see results of some noise reduction concepts reported by Simonich et al.[5] The present studies indicate that accurate representations or computations of the near jet flowfield (where high-frequency noise sources are shown to dominate) are also essential. Because the flow in this region is highly nonequilibrium and anisotropic, turbulence models need to account for the related effects as well.[18] It is evident that significant further developments (in advanced diagnostic experiments closely coupled with modeling) are required for physics-based modeling of aeroacoustics and for its use to evaluate noise reduction concepts.

Acknowledgments

Financial support was provided by corporate internal funding at the United Technologies Research Center. The authors are grateful for stimulating discussions with and insightful comments from B. R. Noack, R. W. Paterson, W. Lord, V. Saxena, and R. H. Schlinker.

References

[1]Tam, C. K. W., "Jet Noise: Since 1952," *Theoretical and Computational Fluid Dynamics*, Vol. 10, 1998, p. 393.

[2]Freund, J. B., "Acoustic Sources in a Turbulent Jet: A Direct Numerical Simulation Study," AIAA Paper 99-1858, May 1999.

[3]Seiner, J. M., "A New Rational Approach to Jet Noise Reduction," *Theoretical and Computational Fluid Dynamics*, Vol. 10, 1998, p. 373.

[4]Bridges, J., and Podboy, G. G., "Measurements of Two-Point Velocity Correlations in a Round Jet with Application to Jet Noise," AIAA Paper 99-1966, May 1999.

[5]Simonich, J., Narayanan, S., Barber, T. J., and Nishimura, M., "High Subsonic Jet Experiments Part 1: Aeroacoustic Characterization, Noise Reduction and Dimensional Scaling Effects," AIAA Paper 2000-2022, June 2000.

[6]Johnson, D. H., and Dudgeon, D. E., *Array Signal Processing: Concepts and Techniques*, Signal Processing Series, Prentice–Hall, Upper Saddle River, NJ, 1993.

[7]Saligrama, V., Polak, D. R., and Narayanan, S., "Phased Array Design, Validation, and Application to Jet Noise Source Localization," AIAA Paper 2000-1934, June 2000.

[8]Papadias, C. B., and Paulraj, A. J., "Space–Time Signal Processing for Wireless Communications: A Survey," *First IEEE Signal Processing Workshop on Signal Processing Advances in Wireless Communications*, Inst. of Electrical and Electronics Engineers, New York, 1997, p. 285.

[9]Fisher, M. J., Harper-Bourne, M., and Glegg, S. A. L., "Jet Engine Noise Source Location: the Polar Correlation Technique," *Journal of Sound and Vibration*, Vol. 51, No. 1, 1977, p. 23.

[10]Bridges, J., "Measurements of Jet Acoustic Source Density," AIAA Paper 99-3787, July 1999.

[11]Ribner, H. S., "Quadrupole Corrections Governing the Pattern of Jet Noise," *Journal of Fluid Mechanics*, Vol. 38, 1969, p. 1.

[12]Lilley, G. M., "On the Noise from Jets," CP-131, AGARD, 1974.

[13]Ahuja, K. K., Massey, K. C., and D'Agostino, M. S., "A Simple Technique of Locating Noise Sources of a Jet Under Simulated Forward Motion," AIAA Paper 98-2359, June 1998.

[14]Hileman, J., Thurow, B., and Samimy, M., "Determination of Noise Sources Within a High-speed Jet via Simultaneous Acoustic Measurements and Real-Time Flow Visualization," AIAA Paper 2001-0374, Jan. 2001.

[15]Bridges, J., and Hussain, F., "Effects of Nozzle Body on Jet Noise," *Journal of Sound and Vibration*, Vol. 188, No. 3, 1995, p. 407.

[16]Lau, J. C., "Effects of Exit Mach Number and Temperature on Mean-Flow and Turbulence Characteristics in Round Jets," *Journal of Fluid Mechanics*, Vol. 105, 1981, p. 193.

[17]Goldstein, M., and Rosenbaum, B., "Effect of Anisotropic Turbulence on Aerodynamic Noise," *Journal of the Acoustical Society of America*, Vol. 54, No. 3, 1973, p. 630.

[18]Khavaran, A., and Krejsa, E. A., "Role of Anisotropy in Turbulent Mixing Noise," AIAA Paper 98-2289, June 1998.

[19]Balsa, T. F., Gliebe, P. R., Kantola, R. A., Mani, R., Stringas, E. J., and Wang, J. C. F., "High Velocity Jet Noise Source Location and Reduction: Task 2-Theoretical Developments and Basic Experiments," Federal Aviation Administration, FAA-RD-76-79-II, May 1978 (available from DTIC as AD A094291).

[20]Tam, C. K. W., and Auriault, L., "Jet Mixing Noise from Fine-Scale Turbulence," *AIAA Journal*, Vol. 37, No. 2, 1999, p. 145.

P. J. Morris
Associate Editor